Communications on Applied Mathematics and Computation
https://doi.org/10.1007/s42967-023-00306-5

ORIGINAL PAPER

A Central Scheme for Two Coupled Hyperbolic Systems

Michael Herty[1] · **Niklas Kolbe**[1] · **Siegfried Müller**[1]

Received: 26 April 2023 / Revised: 29 July 2023 / Accepted: 15 August 2023

Abstract
A novel numerical scheme to solve two coupled systems of conservation laws is introduced. The scheme is derived based on a relaxation approach and does not require information on the Lax curves of the coupled systems, which simplifies the computation of suitable coupling data. The coupling condition for the underlying relaxation system plays a crucial role as it determines the behaviour of the scheme in the zero relaxation limit. The role of this condition is discussed, a consistency concept with respect to the original problem is introduced, the well-posedness is analyzed and explicit, nodal Riemann solvers are provided. Based on a case study considering the p-system of gas dynamics, a strategy for the design of the relaxation coupling condition within the new scheme is provided.

Keywords Coupled conservation laws · Hyperbolic systems · Finite-volume schemes · Coupling conditions · Relaxation system

Mathematics Subject Classification 35L65 · 35R02 · 65M08

1 Introduction

Coupled systems of hyperbolic conservation or balance laws have been discussed in the mathematical literature to address various modelling questions, e.g., regarding two-phase dynamics, multi-scale processes and networks, see, e.g., [12]. The mathematical treatment of interface coupling has been motivated by boundary value problems [2, 16, 25, 31, 32] or by applications to traffic flow on road networks [19, 29], or gas dynamics in large-scale pipelines [5, 6, 14, 53]. It has been further expanded into a well-posedness result for coupled general gas dynamics, see, e.g., [20, 21, 41]. Usually the coupling is imposed at a

✉ Niklas Kolbe
kolbe@igpm.rwth-aachen.de

Michael Herty
herty@igpm.rwth-aachen.de

Siegfried Müller
mueller@igpm.rwth-aachen.de

[1] Institute of Geometry and Applied Mathematics, RWTH Aachen University, Templergraben 55, Aachen 52062, Germany

single spatial interface point as it has been done, e.g., to model production systems [23] and blood flow through systems of blood vessels [27] to mention only a few.

A main challenge has been the derivation of well-posed initial boundary value problems for coupled dynamics out of physically (or problem) induced conditions, see [12] for a recent review. A well-known technique by now is the analytical concept of (half-)Riemann problems [39] or solvers [28]. Moreover, the use of wave-front-tracking techniques yields well-posed coupled problems for a variety of mathematical fluid-type models, see, e.g., [11, 40]. This analytical tool has given rise to the Riemann solver (RS) based numerical methods, which have been proposed, e.g., in [31, 40] and since then extended towards high-order methods [4, 8, 13, 51]. Some high-order methods rely on the linearization of the imposed conditions such that the Lax curves are obtained trivially, see, e.g., [4, 9]. We focus here on finite-volume schemes—finite-element based approaches, such as [26], require a different treatment of coupling conditions. Linearization techniques and Roe-type schemes have been used to avoid the explicit computation of eigenvalues in two-phase problems, see, e.g., [7]. A linearization of the nonlinear dynamics at the coupling point is also at the core of an implicit (in space) numerical scheme [47]. Recently, using projection of the fluxes in the direction normal to the interface an extension of these techniques to the multi-dimensional case has been introduced in [38]. A related problem is given by conservation laws with discontinuous flux at a single point in space. This problem has applications, for instance, in porous media [30], sedimentation processes [15, 24], traffic flow [40] or in supply chain models [35]. In the scalar, one-dimensional case, if conservation of mass and a modified entropy condition across the interface are imposed, solutions are constructed [1] and numerically approximated [3, 50]. A numerical approximation based on relaxation [44] of (scalar) discontinuous fluxes has been proposed in [45]. These schemes, however, rely on analytical expression of Lax curves, which limits those techniques, e.g., when treating phenomena like the multi-phase flow. In various cases such curves are not available [33, 34] or not explicitly given [52].

In this work, a new approach is introduced that does not rely on Lax curves at the interface. Therefore, building on our prior work on scalar equations on networks [36], the nonlinear systems are rewritten in the relaxation form proposed in [44]. Due to the linearity of the relaxed systems, the Lax curves are linearly spanned by the constant eigenvectors of the flux matrix. Based on the reformulation, we derive an explicit scheme for coupled systems of conservation laws by taking a discretization to the zero relaxation limit as suggested also in [44]. The considered coupling differs from the one in [22, 43], where a relaxation system is coupled to a relaxed system. A related approach has been followed in [10], where a kinetic relaxation model governs the coupling conditions. Another alternative is the construction of vanishing viscosity solutions, addressed in the schemes in [46, 55], that avoids the use of Lax curves at the expense of formally treating parabolic systems. The system case that is discussed here requires a detailed analysis of the modified coupling condition imposed to the relaxation formulation, which we will consider.

The outline of this manuscript is as follows: in Sect. 2, we introduce the relaxation form for coupled systems of hyperbolic systems as well as a consistency concept for the corresponding coupling condition. In Sect. 3, we discuss suitable RSs of the coupled problem, discuss their well-posedness, and provide an explicit form for the case of linear coupling conditions. Section 4 is concerned with the construction of a finite-volume scheme for the coupled problem. In Sect. 5, we consider the p-system of gas dynamics in a case study and conduct numerical experiments for different choices of the relaxation coupling condition and then conclude providing a general strategy for the construction of this condition.

2 The Coupled Relaxation System

We consider a coupled system of hyperbolic conservation laws on the real line of the form

$$\begin{cases} \partial_t U + \partial_x F_1(U) = 0, & (t,x) \in (0,\infty) \times (-\infty, 0), \quad (1a) \\ \partial_t U + \partial_x F_2(U) = 0, & (t,x) \in (0,\infty) \times (0,\infty) \quad (1b) \end{cases}$$

with the vector valued state variable $U(t,x) \in \mathbb{R}^n$, and flux functions $F_1, F_2 \colon \mathbb{R}^n \to \mathbb{R}^n$. At the interface located at $x = 0$, a transition between the two flux functions takes place, and we impose the coupling condition

$$\Psi_U(U(t,0^-), U(t,0^+)) = 0 \qquad \text{for a.e. } t > 0, \tag{2}$$

assuming a suitable mapping $\Psi_U \colon \mathbb{R}^n \times \mathbb{R}^n \to \mathbb{R}^m$ for $m \in \mathbb{N}$. To obtain a well-posed problem, a sufficiently large number of suitable conditions are required and thus m depends on the given flux functions. Moreover, we assume initial data given by the vector valued function $U^0(x)$, which is compatible with the coupling condition (2).

The relaxation system [44] was introduced as a dissipative approximation of a hyperbolic system, recovering the original system in the so-called relaxation limit. In this work, we use it as a tool to derive coupling information giving rise to a new method. The relaxation system corresponding to (1) employs the auxiliary state variable $V(t,x) \in \mathbb{R}^n$ and the relaxation rate $\varepsilon > 0$ and reads

$$\begin{cases} \partial_t U + \partial_x V = 0, & (t,x) \in (0,\infty) \times \mathbb{R}\backslash\{0\}, \quad (3a) \\ \partial_t V + A_1\, \partial_x U = \dfrac{1}{\varepsilon}(F_1(U) - V), & (t,x) \in (0,\infty) \times (-\infty, 0), \quad (3b) \\ \partial_t V + A_2\, \partial_x U = \dfrac{1}{\varepsilon}(F_2(U) - V), & (t,x) \in (0,\infty) \times (0,\infty), \quad (3c) \end{cases}$$

where A_1 and A_2 denote diagonal $n \times n$ matrices with positive diagonal entries a_j^i for $j = 1, \cdots, N$ and $i = 1, 2$. These matrices satisfy the subcharacteristic condition

$$A_i - (DF_i(U))^2 \geqslant 0, \qquad i = 1, 2 \tag{4}$$

for all U. This condition has been derived in [49] using the asymptotic analysis. Here, $DF_i(U)$ refers to the Jacobian of F_i in U and the inequality indicates positive semi-definiteness. We note that both U and V depend on ε. Introducing the vector $Q = (U, V)$, we close system (3) using the relaxation coupling condition

$$\Psi_Q(Q(t,0^-), Q(t,0^+)) = 0 \qquad \text{for a.e. } t > 0 \tag{5}$$

for a mapping $\Psi_Q \colon \mathbb{R}^{2n} \times \mathbb{R}^{2n} \to \mathbb{R}^l$, where $l \in \mathbb{N}$. The particular choice of Ψ_Q and m for given Ψ_U is discussed in the following parts of this paper. Initial data for the relaxation system are derived from the original initial data by setting $Q^0 = (U^0, V^0)$ such that

$$V^0(x) = F_1(U^0(x)), \quad \text{if } x < 0, \qquad V^0(x) = F_2(U^0(x)), \quad \text{if } x > 0, \tag{6}$$

and the compatibility of the initial data Q^0 with the coupling condition (5) is assumed.

It is well known that the uncoupled relaxation system recovers the original system of conservation laws as well as $V = F(U)$ as ε tends to zero. We are interested in this relaxation limit at the interface as $\varepsilon \to 0$.

2.1 Continuous Relaxation Limit

The fact that the uncoupled relaxation system tends to a system of conservation laws in the relaxation limit, see [44], raises the question how the coupled systems and, in particular, the coupling conditions (2) and (5) relate. Here we address this question using the asymptotic analysis and suppose that the solution $Q = (U, V)$ of the coupled relaxation system (3) endowed with the coupling condition (5) can be written in terms of a Chapman-Enskog expansion [17], i.e.,

$$Q = \tilde{Q}^0 + \sum_{k=1}^{\infty} \varepsilon^k \tilde{Q}^k. \tag{7}$$

As a solution of the relaxation system in the limit $\varepsilon \to 0$ on both half-axes, the state $\tilde{Q}^0 = (\tilde{U}^0, \tilde{V}^0)$ has the property

$$\tilde{V}^0(t,x) = F_1(\tilde{U}^0(t,x)), \text{ if } x < 0, \qquad \tilde{V}^0(t,x) = F_2(\tilde{U}^0(t,x)), \text{ if } x > 0, \tag{8}$$

and $\tilde{U}^0$ is a solution to the system of conservation laws on both half-axes. If we assume that Ψ_Q is continuously differentiable, we obtain due to the Taylor expansion

$$\Psi_Q(Q(t,0^-), Q(t,0^+)) = \Psi_Q\big(\tilde{Q}^0(t,0^-), \tilde{Q}^0(t,0^+)\big) + \mathcal{O}(\varepsilon), \tag{9}$$

and, in particular, in the limit $\varepsilon \to 0$, we have

$$\Psi_Q\big(\tilde{Q}^0(t,0^-), \tilde{Q}^0(t,0^+)\big) = 0. \tag{10}$$

This observation motivates the following consistency condition.

Definition 1 The coupled relaxation system (3) is *consistent* with the coupled system of conservation laws (1), iff for a.e. $t > 0$, the corresponding coupling conditions (5) and (2) satisfy

$$\Psi_U\big(U(t,0^-), U(t,0^+)\big) = 0, \quad \text{iff} \quad \Psi_Q\left(\begin{pmatrix} U(t,0^-) \\ F_1(U(t,0^-)) \end{pmatrix}, \begin{pmatrix} U(t,0^+) \\ F_2\big(U(t,0^+)\big) \end{pmatrix}\right) = 0. \tag{11}$$

Assuming a smaller number of conditions for the system of conservation laws than for the relaxation system, i.e., $m < l$, this definition implies that consistency requires redundancies occurring in the relaxation limit due to (5).

3 Riemann Solvers (RSs) for the Coupled Relaxation System

In this section, we consider RSs for the coupled relaxation system, which identify coupling data that both solve a half-Riemann problem and satisfy the coupling condition. They are an integral component of the finite-volume schemes introduced in Sect. 4. We introduce the concept in Sect. 3.1, discuss their well-posedness with respect to the coupling condition

in Sect. 3.2, derive an explicit form in the linear case in Sect. 3.3 and study their behaviour in the relaxation limit in Sect. 3.4.

3.1 The Half-Riemann Problem

A finite-volume scheme for a coupled problem such as (3), requires suitable coupling/boundary data, which is obtained by solving a *half-Riemann problem* [25]. Later we will introduce the concept of RSs, which identify coupling data that both solve the half-Riemann problem and satisfy a coupling condition.

To discuss the half-Riemann problem in system (3), we require information about its Lax curves. The relaxation system can be rewritten on both half-axes ($i = 1$, if left, and $i = 2$, if right) as

$$\partial_t Q + S_i\, \partial_x Q = \frac{1}{\varepsilon} \begin{pmatrix} 0 \\ F_i(U) - V \end{pmatrix}, \tag{12}$$

where $S_i \in \mathbb{R}^{2n\times 2n}$ refers to the diagonalizable block matrix

$$S_i = \begin{pmatrix} 0 & I \\ A_i & 0 \end{pmatrix} = \begin{pmatrix} -(\sqrt{A_i})^{-1} & (\sqrt{A_i})^{-1} \\ I & I \end{pmatrix} \begin{pmatrix} -\sqrt{A_i} & 0 \\ 0 & \sqrt{A_i} \end{pmatrix} \begin{pmatrix} -\frac{1}{2}\sqrt{A_i} & \frac{1}{2}I \\ \frac{1}{2}\sqrt{A_i} & \frac{1}{2}I \end{pmatrix} =: R_i \Lambda_i R_i^{-1}. \tag{13}$$

By taking the root of each diagonal entry in A_i, we obtain $\sqrt{A_i}$, which is invertible and satisfies $\sqrt{A_i}\sqrt{A_i} = A_i$. The decomposition (13) shows that the eigenvalues of the system are given by

$$\lambda_j = -\sqrt{a_j^i}, \qquad \lambda_{n+j} = \sqrt{a_j^i} \qquad \text{for } j = 1, \cdots, n. \tag{14}$$

The columns of the matrix R_i include the (right) eigenvectors of the system that can be segmented as

$$R_i = \begin{pmatrix} -(\sqrt{A_i})^{-1} & (\sqrt{A_i})^{-1} \\ I & I \end{pmatrix} =: \begin{pmatrix} R_i^- & R_i^+ \end{pmatrix}, \tag{15}$$

so that $R_i^- \in \mathbb{R}^{2n\times n}$ includes the eigenvectors corresponding to the negative eigenvalues and $R_i^+ \in \mathbb{R}^{2n\times n}$ the ones corresponding to the positive eigenvalues. Analogously, we define the left eigenvectors as the rows of the matrix

$$L_i := R_i^{-1} = \begin{pmatrix} -\frac{1}{2}\sqrt{A_i} & \frac{1}{2}I \\ \frac{1}{2}\sqrt{A_i} & \frac{1}{2}I \end{pmatrix} = \begin{pmatrix} L_i^- \\ L_i^+ \end{pmatrix}, \tag{16}$$

which can again be split with respect to the signs of the corresponding eigenvalues into the matrices $L_i^-, L_i^+ \in \mathbb{R}^{n\times 2n}$. The characteristic variables of the system are

$$\begin{pmatrix} W_i^- \\ W_i^+ \end{pmatrix} := R_i^{-1} Q = \frac{1}{2} \begin{pmatrix} V - \sqrt{A_i} U \\ V + \sqrt{A_i} U \end{pmatrix}. \tag{17}$$

Starting from a state $Q_0^* = (U_0^*, V_0^*)^{\mathrm{T}}$, the Lax curves of the systems are lines in the state space given by

$$\begin{cases} \mathcal{L}_{\lambda_j}(Q_0^*; \sigma_j^-) = Q_0^* - \sigma_j^- (a_j^1)^{-1/2} e_j + \sigma_j^- e_{n+j}, & \text{(18a)} \\ \mathcal{L}_{\lambda_{n+j}}(Q_0^*; \sigma_j^+) = Q_0^* + \sigma_j^+ (a_j^2)^{-1/2} e_j + \sigma_j^+ e_{n+j} & \text{(18b)} \end{cases}$$

for $j = 1, \cdots, n$ with $e_j \in \mathbb{R}^{2n}$ denoting the j-th unit vector and the parameter $\sigma_j^{\pm} \in \mathbb{R}$. Moreover, we define the set

$$\mathcal{L}^-(Q_0^*) := \left\{ Q_0^* + R_1^- \Sigma^- : \ \Sigma^- \in \mathbb{R}^n \right\} = \left\{ \begin{pmatrix} U_0^* - (\sqrt{A_1})^{-1} \Sigma^- \\ V_0^* + \Sigma^- \end{pmatrix} : \ \Sigma^- \in \mathbb{R}^n \right\}, \tag{19a}$$

which includes all states that connect to Q_0^* by Lax curves with negative speeds, i.e., $\mathcal{L}_{\lambda_1}, \cdots, \mathcal{L}_{\lambda_n}$. Conversely, the set of states connecting to Q_0^* by Lax curves with positive speeds, i.e., $\mathcal{L}_{\lambda_{n+1}}, \cdots, \mathcal{L}_{\lambda_{2n}}$, is

$$\mathcal{L}^+(Q_0^*) := \left\{ Q_0^* + R_2^+ \Sigma^+ : \ \Sigma^+ \in \mathbb{R}^n \right\} = \left\{ \begin{pmatrix} U_0^* + (\sqrt{A_2})^{-1} \Sigma^+ \\ V_0^* + \Sigma^+ \end{pmatrix} : \ \Sigma^+ \in \mathbb{R}^n \right\}. \tag{19b}$$

Note that for the following discussion, the Lax curves with negative speeds $\mathcal{L}_{\lambda_1}, \cdots, \mathcal{L}_{\lambda_n}$ in (19) as well as $\mathcal{L}^-$ in (18) are defined for the relaxation system on the left half-axis, whereas the Lax curves with positive speeds $\mathcal{L}_{\lambda_{n+1}}, \cdots, \mathcal{L}_{\lambda_{2n}}$ and $\mathcal{L}^+$ are defined for the relaxation system on the right half-axis.

We consider a situation, where we are given discrete data next to the coupling interface from a finite-volume scheme. We refer to this so-called trace data by $Q_0^- = (U_0^-, V_0^-)$ left from the interface and $Q_0^+ = (U_0^+, V_0^+)$ right from the interface, respectively. We denote boundary/coupling data for the left half-axis $(-\infty, 0)$ by $Q_{\mathrm{R}} = (U_{\mathrm{R}}, V_{\mathrm{R}})$. Analogously, we denote coupling/boundary data for the right half-axis $(0, \infty)$ by $Q_{\mathrm{L}} = (U_{\mathrm{L}}, V_{\mathrm{L}})$. If Q_{R} and Q_{L} constitute a solution of the half-Riemann problem, they need to satisfy

$$Q_{\mathrm{R}} \in \mathcal{L}^-(Q_0^-) \qquad \text{and} \qquad Q_{\mathrm{L}} \in \mathcal{L}^+(Q_0^+). \tag{20}$$

An RS for the relaxation system (3) corresponding to the coupling condition (5) is a mapping

$$\mathcal{RS} : \mathbb{R}^{2n \times 2n} \to \mathbb{R}^{2n \times 2n}, \qquad (Q_0^-, Q_0^+) \mapsto (Q_{\mathrm{R}}, Q_{\mathrm{L}}), \tag{21}$$

that assigns coupling data satisfying the coupling condition and solving the half-Riemann problem to given trace data. It is defined by condition (20) and

$$\Psi_Q(Q_{\mathrm{R}}, Q_{\mathrm{L}}) = 0 \tag{22}$$

for the coupling function introduced in (5). We note that the well-posedness of the RS depends on the coupling condition. The relation between traces, coupling data and coupling condition in the relaxation system is illustrated in Fig. 1.

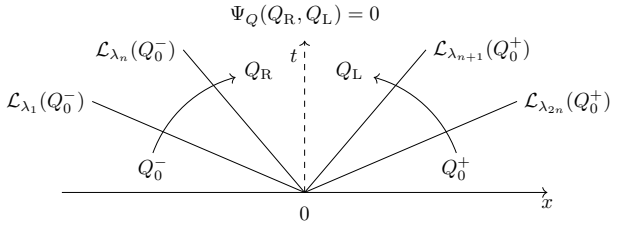

Fig. 1 Wave structure of the coupled relaxation system in the x-t-plane. The left trace data Q_0^- are connected to the coupling data Q_R by the Lax curves of negative speeds, i.e., $\mathcal{L}_{\lambda_1}, \cdots, \mathcal{L}_{\lambda_n}$ and the outgoing trace data Q_0^+ are connected to the coupling data Q_L by the Lax curves of positive speeds, i.e., $\mathcal{L}_{\lambda_{n+1}}, \cdots, \mathcal{L}_{\lambda_{2n}}$. Coupling data on the incoming and outgoing edges are related by the coupling condition Ψ_Q

3.2 Well-Posedness

In this section, we assume general coupling conditions of the form (5) with $l = 2n$, i.e.,

$$\Psi_Q(Q_\mathrm{R}, Q_\mathrm{L}) = 0, \qquad \Psi_Q \colon \mathbb{R}^{2n} \times \mathbb{R}^{2n} \to \mathbb{R}^{2n}. \tag{23}$$

To construct a corresponding RS, we aim to identify coupling data that not only satisfies (23) but also solves the half-Riemann problem (20). Condition (20) allows us to parameterize the coupling data as

$$Q_\mathrm{R}(\Sigma; Q_0) = Q_0^- + R_1^- \Sigma^-, \qquad Q_\mathrm{L}(\Sigma; Q_0) = Q_0^+ + R_2^+ \Sigma^+, \tag{24}$$

using the notation

$$Q_0 = \left(Q_0^-, Q_0^+\right), \quad \Sigma = \left(\Sigma^-, \Sigma^+\right), \tag{25}$$

and thus to introduce the parametrized form of the coupling function

$$\tilde{\Psi}_Q(\Sigma; Q_0) \ := \Psi_Q(Q_\mathrm{R}(\Sigma; Q_0), Q_\mathrm{L}(\Sigma; Q_0)), \qquad \tilde{\Psi}_Q : \mathbb{R}^{2n} \times \mathbb{R}^{4n} \to \mathbb{R}^{2n}. \tag{26}$$

Given this parametrization, we can interpret the $\mathcal{RS}$ (21) for coupling condition (23) as a routine that first identifies Σ by solving the root problem $\tilde{\Psi}_Q(\Sigma; Q_0) = 0$ for given Q_0 and then outputs the data $Q_\mathrm{R}(\Sigma; Q_0)$ and $Q_\mathrm{L}(\Sigma; Q_0)$. It is well posed iff for any trace data Q_0 the equation $\tilde{\Psi}_Q(\Sigma; Q_0) = 0$ has a unique solution $\Sigma = \Xi(Q_0)$. We state a result on its local regularity.

Lemma 1 *Let Ψ_Q be continuously differentiable. Suppose that for a fixed $Q_0 \in \mathbb{R}^{4n}$, there is a unique $\Sigma \in \mathbb{R}^{2n}$ satisfying $\tilde{\Psi}_Q(\Sigma; Q_0) = 0$ and the Jacobian $D_\Sigma \tilde{\Psi}_Q(\Sigma; Q_0)$ is invertible. Then there is an open ball $B_{Q_0} \subset \mathbb{R}^{4n}$ around Q_0 such that the $\mathcal{RS}$ (21) with coupling condition (23) is well defined and continuously differentiable for all $\tilde{Q}_0 = (\tilde{Q}_0^-, \tilde{Q}_0^+)^\mathrm{T} \in B_{Q_0}$.*

Proof Due to the implicit function theorem, there are open balls B_Σ and B_{Q_0} around Σ and Q_0, respectively, and a unique continuously differentiable mapping $\Xi \colon B_{Q_0} \to B_\Sigma$ such that

$$\tilde{\Psi}_Q(\tilde{\Sigma}; \tilde{Q}_0) = 0, \quad \text{iff} \quad \tilde{\Sigma} = \Xi(\tilde{Q}_0) \tag{27}$$

for all $\tilde{Q}_0 \in B_{Q_0}$ and $\tilde{\Sigma} \in B_\Sigma$. The statement is obtained taking into account that the output of the $\mathcal{RS}$ (21) is uniquely given by $Q_\mathrm{R}(\Xi(\tilde{Q}_0); \tilde{Q}_0)$ and $Q_\mathrm{L}(\Xi(\tilde{Q}_0); \tilde{Q}_0)$ for all $\tilde{Q}_0 \in B_{Q_0}$.

A further result is obtained applying the contraction mapping theorem to a fixed point iteration of the form

$$\Sigma^{n+1} = \Sigma^n - A(Q_0)\tilde{\Psi}_Q(\Sigma^n; Q_0) \tag{28}$$

with $A(Q_0) \in \mathbb{R}^{2n\times 2n}$ invertible.

Lemma 2 *Let $\mathcal{S} \subset \mathbb{R}^{4n}$ and $\mathcal{P} \subset \mathbb{R}^{2n}$ denote open sets. Suppose that for any $Q_0 \in \mathcal{S}$, there is a regular matrix $A(Q_0) \in \mathbb{R}^{2n\times 2n}$ such that*

$$T_{Q_0}(\Sigma) = \Sigma - A(Q_0)\tilde{\Psi}_Q(\Sigma; Q_0) \in \mathcal{P} \tag{29}$$

for all $\Sigma \in \mathcal{P}$ and T_{Q_0} is Lipschitz continuous with the Lipschitz constant $K < 1$. Then $\mathcal{RS}$: $\mathcal{S} \to \mathbb{R}^{2n} \times \mathbb{R}^{2n}$ defined through (20), (21), and (23) is well defined.

Proof For $Q_0 \in \mathcal{S}$, the function $T_{Q_0}(\Sigma)$ maps from $\mathcal{P}$ to $\mathcal{P}$ due to (29) and is a contraction mapping as it is Lipschitz continuous with sufficiently small Lipschitz constant. Thus, by the contraction mapping theorem, the sequence (28) admits for any arbitrary $\Sigma^0 \in \mathcal{P}$ a unique fixed point $\tilde{\Sigma}$ satisfying $\tilde{\Psi}_Q(\tilde{\Sigma}; Q_0) = 0$. This implies the well-posedness of $\mathcal{RS}_{\tilde{\Psi}_Q}$.

Remark 1 The Lipschitz continuity of T_{Q_0} in Lemma 2 is implied by the stronger condition

$$\sup_{\Sigma\in\mathcal{P}} \|I - A(Q_0)D_\Sigma\tilde{\Psi}_Q(Q_0; \Sigma)\| < 1. \tag{30}$$

We note that Lemmas 1 and 2 allow to freely choose the vector norm in $\mathbb{R}^n$ determining the induced matrix norm in Remark 1.

3.3 Linear Coupling Conditions

In this section, we discuss a special case of (23), namely affine linear coupling functions of the form

$$\Psi_Q(Q_\mathrm{R}, Q_\mathrm{L}) = B_\mathrm{R}Q_\mathrm{R} - B_\mathrm{L}Q_\mathrm{L} - P \tag{31}$$

for $B_\mathrm{R}, B_\mathrm{L} \in \mathbb{R}^{2n\times 2n}$ and $P \in \mathbb{R}^{2n}$. Under further conditions on the matrices, we can provide explicit formulas of the coupling data obtained by the corresponding $\mathcal{RS}$ (21). We introduce the block matrices

$$\tilde{R}^- = \begin{pmatrix} R_1^- & 0 \end{pmatrix} = \begin{pmatrix} -(\sqrt{A_1})^{-1} & 0 \\ I & 0 \end{pmatrix}, \qquad \tilde{R}^+ = \begin{pmatrix} 0 & R_2^+ \end{pmatrix} = \begin{pmatrix} 0 & (\sqrt{A_2})^{-1} \\ 0 & I \end{pmatrix} \tag{32}$$

satisfying $\tilde{R}^-\Sigma = R_1^-\Sigma^-$ and $\tilde{R}^+\Sigma = R_2^+\Sigma^+$ assuming definition (25).

Proposition 1 *Suppose the matrix $B_R\tilde{R}^- - B_L\tilde{R}^+$ is regular. Then the RS corresponding to the affine linear coupling function (31) is well defined and yields the output*

$$Q_R = Q_0^- + \tilde{R}^- \Sigma, \qquad Q_L = Q_0^+ + \tilde{R}^+ \Sigma, \tag{33}$$

where Σ is the unique solution of the linear system

$$\left(B_R\tilde{R}^- - B_L\tilde{R}^+\right)\Sigma = P + B_L Q_0^+ - B_R Q_0^-. \tag{34}$$

Proof Using the parametrization (24), we rewrite the coupling condition as

$$0 = \Psi_Q(Q_R(\Sigma; Q_0), Q_L(\Sigma; Q_0)) = B_R\left(Q_0^- + \tilde{R}^-\Sigma\right) - B_L\left(Q_0^+ + \tilde{R}^+\Sigma\right) - P,$$

which implies (34).

In case of block matrices, the system (34) can be solved using a block LU decomposition.

Remark 2 Suppose the matrices B_R and B_L are given in a block form as

$$B_R = \begin{pmatrix} B_R^{11} & B_R^{12} \\ B_R^{21} & B_R^{22} \end{pmatrix}, \qquad B_L = \begin{pmatrix} B_L^{11} & B_L^{12} \\ B_L^{21} & B_L^{22} \end{pmatrix} \tag{35}$$

with each block being a matrix in $\mathbb{R}^{n\times n}$. The system matrix in (34) then takes the form

$$B_R\tilde{R}^- - B_L\tilde{R}^+ = \begin{pmatrix} B_R^{12} - B_R^{11}(\sqrt{A_1})^{-1} & -B_L^{12} - B_L^{11}(\sqrt{A_2})^{-1} \\ B_R^{22} - B_R^{21}(\sqrt{A_1})^{-1} & -B_L^{22} - B_L^{21}(\sqrt{A_2})^{-1} \end{pmatrix} =: \begin{pmatrix} B^{11} & B^{12} \\ B^{21} & B^{22} \end{pmatrix} = B. \tag{36}$$

Suppose now that B^{11} and $S := B^{22} - B^{21}(B^{11})^{-1}B^{12}$ are regular, then the RS corresponding to the coupling condition (31) is well defined and coupling data can be computed using the inverse system matrix

$$B^{-1} = \begin{pmatrix} (B^{11})^{-1}\left(I + B^{12}S^{-1}B^{21}(B^{11})^{-1}\right) & -(B^{11})^{-1}B^{12}S^{-1} \\ -SB^{21}(B^{11})^{-1} & S^{-1} \end{pmatrix}. \tag{37}$$

If B^{11} in Remark 2 is not regular, a block LU decomposition of B and an inverse matrix similar to (37) might still be computable after suitable rotation of the rows and columns.

Note that assuming the coupling condition (31), the relaxation system (5) is consistent (in the sense of Definition 1) with system (1), if $\Psi_U(U_R, U_L) = 0$ is equivalent to

$$B_R\begin{pmatrix} U_R \\ F_1(U_R) \end{pmatrix} - B_L\begin{pmatrix} U_L \\ F_2(U_L) \end{pmatrix} - P = 0. \tag{38}$$

Example 1 (Kirchhoff conditions) A canonical choice of coupling conditions for (3) is the ones due to Kirchhoff, which requires equality of the fluxes left and right from the interface, in all equations of the system, i.e.,

$$\Psi_Q^K(Q_R, Q_L) = S_1 Q_R - S_2 Q_L = 0. \tag{39}$$

By choosing the diagonal entries sufficiently large (such that (4) holds), we can achieve $A_1 = A_2 =: A$, which we assume in the following. Consequently, the quantities in (13), (17), and (19) are independent of the half-axis considered and we therefore neglect the index i. Since S is regular, the coupling condition (39) simplifies to

$$\Psi_Q^K(Q_\mathrm{R}, Q_\mathrm{L}) = Q_\mathrm{R} - Q_\mathrm{L} = 0, \tag{40}$$

and thus the coupling function is of the form (31) for $B_\mathrm{R} = B_\mathrm{L} = I$ and $P = 0$.

From (34), we obtain

$$\begin{pmatrix} -\Sigma^- \\ \Sigma^+ \end{pmatrix} = \begin{pmatrix} R^- & R^+ \end{pmatrix}^{-1} (Q_0^- - Q_0^+) = \begin{pmatrix} L^- \\ L^+ \end{pmatrix} (Q_0^- - Q_0^+),$$

and consequently the coupling data is given by

$$Q_\mathrm{R} = Q_0^- - R^- L^- (Q_0^- - Q_0^+), \quad Q_\mathrm{R} = Q_0^+ + R^+ L^+ (Q_0^- - Q_0^+),$$

or equivalently,

$$\begin{cases} U_\mathrm{R} = U_\mathrm{L} = \dfrac{1}{2}(U_0^- + U_0^+) + \dfrac{1}{2}(\sqrt{A})^{-1}(V_0^- - V_0^+), & \text{(41a)} \\ V_\mathrm{R} = V_\mathrm{L} = \dfrac{1}{2}(V_0^- + V_0^+) + \dfrac{1}{2}\sqrt{A}(U_0^- - U_0^+). & \text{(41b)} \end{cases}$$

The relation between trace and coupling data inferred by (20) and (40) therefore defines an RS with easy-to-compute coupling data. In general the coupling condition (39) does not lead to the consistency with the original Kirchhoff coupling problem, in which (1) is endowed with the coupling condition

$$\Psi_U^K(U(t,0^-), U(t,0^+)) = F_1(U(t,0^-)) - F_2(U(t,0^+)) = 0.$$

This is due to the lower n components in (39) that in general impose additional conditions in the relaxation limit. Instead concluding from (38) the consistency requires that $\Psi_U(U(t,0^-), U(t,0^+)) = 0$ holds iff

$$U(t,0^-) - U(t,0^+) = F_1(U(t,0^-)) - F_2(U(t,0^+)) = 0.$$

3.4 Discrete Relaxation Limit

Similarly as for the continuous problem in Sect. 2.1, we can analyze the relaxation limit of the RS. Therefore, we assume that the trace data $Q_0 = (Q_0^-, Q_0^+)$ can be asymptotically expanded around the state $Q_0^0 = \left(Q_0^{0,-}, Q_0^{0,+}\right)$ as

$$Q_0^- = Q_0^{0,-} + \sum_{k=1}^{\infty} \varepsilon^k Q_0^{k,-}, \qquad Q_0^+ = Q_0^{0,+} + \sum_{k=1}^{\infty} \varepsilon^k Q_0^{k,+}. \tag{42}$$

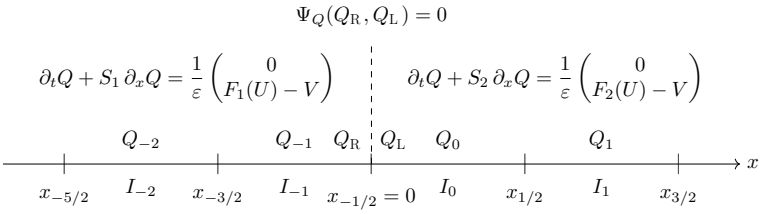

Fig. 2 The relaxation system in the 1-to-1 coupling case on the discretized real line

Moreover, we assume in analogy to Lemma 1 that Ψ_Q is continuously differentiable and that for all Q_0 there is a unique $(\Sigma^-(Q_0), \Sigma^+(Q_0)) = \Sigma \in \mathbb{R}^{2n}$ satisfying $\tilde{\Psi}_Q(\Sigma; Q_0) = 0$ and the Jacobian $D_\Sigma \tilde{\Psi}_Q(\Sigma; Q_0)$ is invertible. From the parametrization (24), we obtain

$$Q_\mathrm{R}(\Sigma; Q_0) = Q_0^- + R_1^- \Sigma^-(Q_0), \qquad Q_\mathrm{L}(\Sigma; Q_0) = Q_0^+ + R_2^+ \Sigma^+(Q_0). \tag{43}$$

Due to the implicit function theorem, see the proof of Lemma 1, Σ^- and Σ^+ are continuously differentiable functions in Q_0 and by the Taylor expansion,

$$\Sigma^\mp(Q_0) = \Sigma^\mp(Q_0^0) + \mathcal{O}(\varepsilon) \tag{44}$$

holds. Hence, we obtain by substitution in (43)

$$Q_\mathrm{R}(\Sigma; Q_0) = Q_0^{0,-} + R_1^- \Sigma^-\left(Q_0^0\right) + \mathcal{O}(\varepsilon), \quad Q_\mathrm{L}(\Sigma; Q_0) = Q_0^{0,+} + R_2^+ \Sigma^+\left(Q_0^0\right) + \mathcal{O}(\varepsilon), \tag{45}$$

or, in different terms

$$\mathcal{RS}(Q_0^-, Q_0^+) = \mathcal{RS}\left(Q_0^{0,-}, Q_0^{0,+}\right) + \mathcal{O}(\varepsilon). \tag{46}$$

Using a Taylor expansion of Ψ_Q, we further see that

$$\Psi_Q(Q_\mathrm{R}(\Sigma(Q_0); Q_0), Q_\mathrm{L}(\Sigma(Q_0); Q_0)) = \Psi_Q(Q_\mathrm{R}(\Sigma(Q_0^0); Q_0^0), Q_\mathrm{L}(\Sigma(Q_0^0); Q_0^0)) + \mathcal{O}(\varepsilon),$$

and thus, in the limit $\varepsilon \to 0$, the coupling data satisfy the coupling condition, i.e.,

$$\Psi_Q(Q_\mathrm{R}(\Sigma(Q_0^0); Q_0^0), Q_\mathrm{L}(\Sigma(Q_0^0); Q_0^0)) = 0. \tag{47}$$

4 The Central Scheme

We consider a discretization of the real line into uniform mesh cells $I_j = (x_{j-1/2}, x_{j+1/2})$ of width Δx with origin located at the cell interface $x_{-1/2}$ as indicated by Fig. 2. Furthermore, the time line is partitioned into the instances $t^n = \sum_{k=1}^n \Delta t^n$ for some time increments $\Delta t^n > 0$, which for brevity we assume uniform and denote by Δt throughout this section. Let Q_j^n, U_j^n, and V_j^n denote piecewise constant numerical solutions of system (3) in terms of cell averages over cell I_j at time t^n.

4.1 Relaxation Scheme

An asymptotic preserving scheme for the coupled relaxation system (3) and coupling condition (5) is obtained by combining the first-order upwind discretization with an implicit-explicit time discretization as in [36, 42]. The scheme takes the form

$$\begin{cases} U_j^{n+1} = U_j^n - \dfrac{\Delta t}{\Delta x}\left(F_{j+1/2}^{n,-} - F_{j-1/2}^{n,+}\right), & \text{(48a)} \\ V_j^{n+1} = V_j^n - \dfrac{\Delta t}{\Delta x}\left(G_{j+1/2}^{n,-} - G_{j-1/2}^{n,+}\right) + \dfrac{\Delta t}{\varepsilon}\left(F_i(U_j^{n+1}) - V_j^{n+1}\right), & \text{(48b)} \end{cases}$$

where $i = 1$, if $j < 0$, and $i = 2$, if $j \geqslant 0$. We distinguish between incoming numerical fluxes from the left cell interface (indicated by a plus sign) and numerical fluxes outgoing through the right cell interface (indicated by a minus sign). Away from the coupling interface, they are equal as we have

$$\begin{cases} F_{j-1/2}^{n,+} = F_{j-1/2}^{n,-} = \dfrac{1}{2}\left(V_{j-1}^n + V_j^n\right) - \dfrac{1}{2}\sqrt{A_i}(U_j^n - U_{j-1}^n), & \text{(49a)} \\ G_{j-1/2}^{n,+} = G_{j-1/2}^{n,-} = \dfrac{1}{2}A_i(U_{j-1}^n + U_j^n) - \dfrac{1}{2}\sqrt{A_i}(V_j^n - V_{j-1}^n) & \text{(49b)} \end{cases}$$

for $j \in \mathbb{Z}\backslash\{0\}$ and i chosen according to the sign of j as in (48). At the interface, the scheme is not necessarily conservative since the numerical fluxes are given by

$$\begin{cases} F_{-1/2}^{n,-} = \dfrac{1}{2}\left(V_{-1}^n + V_{\mathrm{R}}^n\right) - \dfrac{1}{2}\sqrt{A_1}(U_{\mathrm{R}}^n - U_{-1}^n), & \text{(49c)} \\ F_{-1/2}^{n,+} = \dfrac{1}{2}\left(V_{\mathrm{L}}^n + V_0^n\right) - \dfrac{1}{2}\sqrt{A_2}(U_0^n - U_{\mathrm{L}}^n), & \text{(49d)} \\ G_{-1/2}^{n,-} = \dfrac{1}{2}A_1(U_{-1}^n + U_{\mathrm{R}}^n) - \dfrac{1}{2}\sqrt{A_1}(V_{\mathrm{R}}^n - V_{-1}^n), & \text{(49e)} \\ G_{-1/2}^{n,+} = \dfrac{1}{2}A_2(U_{\mathrm{L}}^n + U_0^n) - \dfrac{1}{2}\sqrt{A_2}(V_0^n - V_{\mathrm{L}}^n). & \text{(49f)} \end{cases}$$

The discrete coupling data employed in the numerical fluxes (49c)–(49f) are obtained applying the RS from Sect. 3 to the cell averages adjacent to the interface, i.e.,

$$\mathcal{RS}((U_{-1}^n, V_{-1}^n), (U_0^n, V_0^n)) =: ((U_{\mathrm{R}}^n, V_{\mathrm{R}}^n), (U_{\mathrm{L}}^n, V_{\mathrm{L}}^n)). \tag{50}$$

4.2 Relaxed Scheme

In this section, using the asymptotic analysis as done in Sects. 2.1 and 3.4, we consider the relaxation limit of the relaxation scheme. The cell averages U_j^n and V_j^n occurring in the schemes above depend on the relaxation rate ε. We assume that for all j and n, they can be

asymptotically expanded around the zero relaxation states $U_j^{n,0}$ and $V_j^{n,0}$ for sufficiently small relaxation rates as

$$\begin{cases} U_j^n = U_j^{n,0} + \varepsilon U_j^{n,1} + \mathcal{O}(\varepsilon^2), & \text{(51a)} \\ V_j^n = V_j^{n,0} + \varepsilon V_j^{n,1} + \mathcal{O}(\varepsilon^2). & \text{(51b)} \end{cases}$$

At first, we consider the relaxation limit away from the interface. We fix $j \in \mathbb{Z}\backslash\{-1,0\}$ and choose i according to the sign of j as in (48), and then substitute the expansions (51) into (48b). After the Taylor expansion, we obtain

$$\begin{aligned} V_j^{n+1,0}\left(1+\frac{\Delta t}{\varepsilon}\right) = V_j^{n,0} - \frac{\Delta t}{\Delta x}\left(G_{j+1/2}^{n,+,0} - G_{j-1/2}^{n,-,0}\right) \\ + \frac{\Delta t}{\varepsilon}\left(F_i(U_j^{n+1,0}) + \varepsilon DF_i(U_j^{n+1,0})\, U_j^{n+1,1} - \varepsilon V_j^{n,1}\right) + \mathcal{O}(\varepsilon), \end{aligned} \tag{52}$$

where DF_i denotes the Jacobian of F_i, and $G_{j-1/2}^{n,\mp,0} = G_{j-1/2}^{n,\mp,0}\left((U_{j-1}^{n,0}, U_{j-1}^{n,0}), (U_j^{n,0}, U_j^{n,0})\right)$, the numerical flux equivalents to (49b) at the zero relaxation state. Due to the expansion

$$\left(1+\frac{\Delta t}{\varepsilon}\right)^{-1} = \frac{\varepsilon}{\varepsilon+\Delta t} = \frac{\varepsilon}{\Delta t} + \mathcal{O}(\varepsilon^2), \tag{53}$$

we obtain by multiplication in (52)

$$V_j^{n+1,0} = F_i(U_j^{n+1,0}) + \mathcal{O}(\varepsilon) \qquad \text{for all } n \in \mathbb{N}_0. \tag{54}$$

Substituting now the asymptotic expansion (51) into (48a) and taking into account (54), we obtain

$$U_j^{n+1,0} = U_j^{n,0} - \frac{\Delta t}{\Delta x}\left(F_{j+1/2}^{n,+,0} - F_{j-1/2}^{n,-,0}\right) + \mathcal{O}(\varepsilon), \tag{55}$$

where the numerical fluxes take the form

$$F_{j-1/2}^{n,+,0} = F_{j-1/2}^{n,-,0} = \frac{1}{2}\left(F_i(U_{j-1}^{n,0}) + F_i(U_j^{n,0})\right) - \frac{1}{2}\sqrt{A_i}(U_j^{n,0} - U_{j-1}^{n,0}). \tag{56}$$

In the relaxation limit, the $\mathcal{O}(\varepsilon)$ terms in (54) and (55) vanish, which gives rise to the relaxed scheme on both half-axes.

Next, we investigate the relaxation limit at the interface. We assume that in case of the asymptotic expansion (51), the $\mathcal{RS}$ (21) satisfies

$$\mathcal{RS}((U_{-1}^n, V_{-1}^n), (U_0^n, V_0^n)) = \mathcal{RS}_0((U_{-1}^{n,0}, V_{-1}^{n,0}), (U_0^{n,0}, V_0^{n,0})) + \mathcal{O}(\varepsilon) \tag{57}$$

for some mapping

$$\mathcal{RS}_0 \colon \mathbb{R}^{2n} \times \mathbb{R}^{2n} \to \mathbb{R}^{2n} \times \mathbb{R}^{2n}.$$

In Sect. 3.4, we have shown that under suitable conditions on Ψ_Q condition (57) holds for $\mathcal{RS}_0 = \mathcal{RS}$, i.e., the coupling in the limit is determined by the original $\mathcal{RS}$. We note, however, that in general $\mathcal{RS}_0$ may not necessarily be a $\mathcal{RS}$ in the sense, it was introduced in Sect. 3.1.

Condition (57) allows us to define the limit coupling data

$$\mathcal{RS}_0((U_{-1}^{n,0}, V_{-1}^{n,0}), (U_0^{n,0}, V_0^{n,0})) =: ((U_{\mathrm{R}}^{n,0}, V_{\mathrm{R}}^{n,0}), (U_{\mathrm{L}}^{n,0}, V_{\mathrm{L}}^{n,0})), \tag{58}$$

and therefore also the interface fluxes

$$\begin{cases} F_{-1/2}^{n,-,0} = \frac{1}{2}(V_{-1}^{n,0} + V_{\mathrm{R}}^{n,0}) - \frac{1}{2}\sqrt{A_1}(U_{\mathrm{R}}^{n,0} - U_{-1}^{n,0}), & \text{(59a)} \\ F_{-1/2}^{n,+,0} = \frac{1}{2}(V_{\mathrm{L}}^{n,0} + V_0^{n,0}) - \frac{1}{2}\sqrt{A_2}(U_0^{n,0} - U_{\mathrm{L}}^{n,0}), & \text{(59b)} \\ G_{-1/2}^{n,-,0} = \frac{1}{2}A_1(U_{-1}^{n,0} + U_{\mathrm{R}}^{n,0}) - \frac{1}{2}\sqrt{A_1}(V_{\mathrm{R}}^{n,0} - V_{-1}^{n,0}), & \text{(59c)} \\ G_{-1/2}^{n,+,0} = \frac{1}{2}A_2(U_{\mathrm{L}}^{n,0} + U_0^{n,0}) - \frac{1}{2}\sqrt{A_2}(V_0^{n,0} - V_{\mathrm{L}}^{n,0}). & \text{(59d)} \end{cases}$$

Combining these fluxes with the above arguments and using assumption (57), it is now straightforward to show that (54) and (55) also hold for $j = -1$ and $j = 0$. Eventually, we take the relaxation limit $\varepsilon \to 0$, drop the index 0 and obtain the *coupled relaxed* or *central scheme* for system (3) and coupling condition (5) in the relaxation limit, which reads

$$U_j^{n+1} = U_j^n - \frac{\Delta t}{\Delta x}\left(H_{j+1/2}^{n,-} - H_{j-1/2}^{n,+}\right) \quad \text{for all } j \in \mathbb{Z}, \tag{60a}$$

and employs the numerical fluxes

$$H_{j-1/2}^{n,+} = H_{j-1/2}^{n,-} = \frac{1}{2}(F_i(U_{j-1}^n) + F_i(U_j^n)) - \frac{1}{2}\sqrt{A_i}(U_j^n - U_{j-1}^n) \tag{60b}$$

for $j \in \mathbb{Z}\backslash\{0\}$ and i chosen according to the sign of j. At the interface, we have

$$H_{-1/2}^{n,-} = \frac{1}{2}(F_1(U_{-1}^n) + V_{\mathrm{R}}^n) - \frac{1}{2}\sqrt{A_1}(U_{\mathrm{R}}^n - U_{-1}^n), \tag{60c}$$

$$H_{-1/2}^{n,+} = \frac{1}{2}(V_{\mathrm{L}}^n + F_2(U_0^n)) - \frac{1}{2}\sqrt{A_2}(U_0^n - U_{\mathrm{L}}^n), \tag{60d}$$

where the variables $V_{\mathrm{R}}^n = V_{\mathrm{R}}^n(U_{-1}^n, U_0^n)$, $V_{\mathrm{L}}^n = V_{\mathrm{L}}^n(U_{-1}^n, U_0^n)$ depend only on the cell averages of the state variable next to the interface as part of the coupling data

$$\mathcal{RS}_0((U_{-1}^n, F_1(U_{-1}^n)), (U_0^n, F_2(U_0^n))) =: ((U_{\mathrm{R}}^n, V_{\mathrm{R}}^n), (U_{\mathrm{L}}^n, V_{\mathrm{L}}^n)). \tag{60e}$$

Remark 3 Suppose that Ψ_Q is continuously differentiable, for all Q_0, there is a unique $\Sigma \in \mathbb{R}^n$ satisfying $\tilde{\Psi}_Q(\Sigma; Q_0) = 0$ and the Jacobian $D_\Sigma \tilde{\Psi}_Q(\Sigma; Q_0)$ is invertible. Then following from Sect. 3.4, the RS for the coupling condition (23) is well defined and $\mathcal{RS}_0 := \mathcal{RS}$ satisfies (57) and defines a limit scheme.

Example 2 If Kirchhoff conditions are assumed for Ψ_Q together with $A_1 = A_2 = A$ as discussed in Example 1, we can substitute the explicit formulas of the coupling data and obtain a conservative scheme of the form (60a) with the numerical fluxes

$$H^{n,+}_{j-1/2} = H^{n,-}_{j-1/2} = \begin{cases} \frac{1}{2}\left(F_1(U^n_{j-1}) + F_1(U^n_j)\right) - \frac{1}{2}\sqrt{A}(U^n_j - U^n_{j-1}), & \text{if } j < 0, \\ \frac{1}{2}\left(F_1(U^n_{-1}) + F_2(U^n_0)\right) - \frac{1}{2}\sqrt{A}(U^n_0 - U^n_{-1}), & \text{if } j = 0, \\ \frac{1}{2}\left(F_2(U^n_{j-1}) + F_2(U^n_j)\right) - \frac{1}{2}\sqrt{A}(U^n_j - U^n_{j-1}), & \text{if } j > 0. \end{cases} \tag{61}$$

This follows from generalizing the scalar approach in [36] to the system case.

5 Case Study: the *p*-System

In this section, we apply the developed approach to a problem arising in gas transportation networks considered in [38]. Motivated by recent significant increases of gas-fired electrical generation in parts of the USA, see, e.g., [56], the modelling of high-pressure gas transportation networks needs to account for the influence of gas-fired power generators. The gas flow through pipelines has been effectively modelled using the compressible Euler equations [14]. Neglecting temperature dynamics, the p-system is used as a simplified model of gas dynamics, see, e.g., [37], given by

$$\partial_t \rho + \partial_x(\rho v) = 0, \tag{62a}$$

$$\partial_t(\rho v) + \partial_x(\rho v^2 + p(\rho)) = 0, \tag{62b}$$

and accounting for the conservation of density ρ and momentum ρv. As closure for the system, we impose the γ-law for the pressure function

$$p(\rho) = \alpha \rho^\gamma \tag{62c}$$

with parameters $\alpha > 0$ and $\gamma > 0$. To account for the gas-fired power generation, we consider (62) on both real half-axes coupled at an interface located at $x = 0$ in analogy to (1). In this setting, a gas turbine acting as the power generator is assumed at the interface. The impact of the turbine on the gas network is modeled by conditions that leave the pressure of the transmitted gas constant but account for a loss in momentum [18], giving rise to the coupling conditions

$$\rho_{\mathrm{R}} v_{\mathrm{R}} = \rho_{\mathrm{L}} v_{\mathrm{L}} + \mathcal{E}, \tag{63a}$$

$$p(\rho_{\mathrm{R}}) = p(\rho_{\mathrm{L}}), \tag{63b}$$

which govern the coupling function Ψ_U. In condition (63a), the parameter $\mathcal{E} \leqslant 0$ controls the mass outtake due to the turbine. As the density ρ is assumed nonnegative, we note that condition (63b), imposing continuity of the pressure at the interface, is equivalent to

$$\rho_{\mathrm{R}} = \rho_{\mathrm{L}}. \tag{64}$$

5.1 Relaxation Form

Introducing the two auxiliary scalar variables V_1, V_2 and the relaxation rate ε, the relaxation system corresponding to the coupled p-system (62) takes the form

$$\begin{cases} \partial_t \rho + \partial_x(V_1) = 0, & (65a) \\ \partial_t(\rho v) + \partial_x(V_2) = 0, & (65b) \\ \partial_t V_1 + a\partial_x \rho = \dfrac{1}{\varepsilon}(\rho v - V_1), & (65c) \\ \partial_t V_2 + a\partial_x(\rho v) = \dfrac{1}{\varepsilon}(\rho v^2 + p(\rho) - V_2). & (65d) \end{cases}$$

As system (62) also its relaxation variant (65) is imposed on both real half-axes coupled at an interface located at $x = 0$. Compared to the general relaxation form (3), the parameters a_i^j are chosen independent of both the half-axis and the system component and set to the square of the maximal speed of sound, i.e.,

$$a = \max_{\rho \in [0, \rho^{\max}]} p'(\rho).$$

This choice is motivated by the fact that $\sqrt{p'(\rho)}$ is a good approximation for the maximal eigenvalue of the p-system. In vector form, system (65) uses the variables $U = (\rho, \rho v)$ and $V = (V_1, V_2)$ and the matrix $A = aI$.

We are interested in identifying a suitable coupling function Ψ_Q for the coupled relaxation system (65). The implied condition should be such that in the limit $\varepsilon \to 0$, the dynamics of the original coupled p-system given by (62) and (63) are attained. At first, we look at linear coupling conditions of the type

$$\begin{cases} \rho_{\mathrm{R}} = \rho_{\mathrm{L}}, & (66a) \\ \rho_{\mathrm{R}} v_{\mathrm{R}} = \rho_{\mathrm{L}} v_{\mathrm{L}} + \beta_1 \mathcal{E}, & (66b) \\ V_{1\mathrm{R}} = V_{1\mathrm{L}} + \beta_2 \mathcal{E}, & (66c) \\ V_{2\mathrm{R}} = V_{2\mathrm{L}} & (66d) \end{cases}$$

for $\beta_1, \beta_2 \in \{0, 1\}$. As approach 1 motivated from (63a) and (64), we consider the case $\beta_1 = 1$ and $\beta_2 = 0$. The conditions (66c) (with $\beta_2 = 0$) and (66d) for the auxiliary variable V have been chosen assuming continuity of the auxiliary variable. Noting that in the relaxation limit, it holds $V_1 = \rho v$, the jump condition (63a) can also be implemented in (66c). This motivates our approach 2, for which we choose $\beta_1 = 0$ and $\beta_2 = 1$. Our approach 3 combines the two former ones by setting $\beta_1 = \beta_2 = 1$.

By our analysis in Sect. 2.1 and the linearity of the coupling approaches 1–3, the auxiliary variables satisfy in the relaxation limit

$$V_{1\mathrm{R}} = \rho_{\mathrm{R}} v_{\mathrm{R}}, \quad V_{1\mathrm{L}} = \rho_{\mathrm{L}} v_{\mathrm{L}}, \quad V_{2\mathrm{R}} = \rho_{\mathrm{R}}(v_{\mathrm{R}})^2 + p(\rho_{\mathrm{R}}), \quad V_{2\mathrm{L}} = \rho_{\mathrm{L}}(v_{\mathrm{L}})^2 + p(\rho_{\mathrm{L}}). \quad (67)$$

This limit condition shows that both our first and second coupling approaches for system (65) lead to a contradiction in (66b) and (66c) in the relaxation limit due to $\beta_1 \neq \beta_2$.

Our third approach corrects this. However, due to (66d), this approach as well as the two former ones impose a condition in the limit that is not implied by the original coupling condition (63). In more details, this additional condition imposes $v_R = v_L$, whenever $\rho_R v_R = \rho_L v_L \neq 0$. Consequently, our three coupling approaches within (66) cannot lead to consistency of the relaxation system (66) with the p-system (62) and coupling condition (63) in the sense of Definition 1.

We aim to design a coupling condition that leads to consistency by taking our third approach as a starting point and deriving a suitable replacement for condition (66d). Therefore, we assume (63a), (64) as well as $\rho_R = \rho_L \neq 0$ and find

$$\rho_R v_R^2 + p(\rho_R) = \frac{\rho_R^2 v_R^2}{\rho_R} + p(\rho_R) = \frac{(\rho_L v_L + \mathcal{E})^2}{\rho_R} + p(\rho_L) = \rho_L v_L^2 + p(\rho_L) + \mathcal{E}\,\frac{2\rho_L v_L + \mathcal{E}}{\rho_L}. \tag{68}$$

This motivates the new condition

$$V_{2R} = V_{2L} + \mathcal{E}\,\frac{2\rho_L v_L + \mathcal{E}}{\rho_L}, \tag{69}$$

which together with (66a), (66b), (66c) and $\beta_1 = \beta_2 = 1$ determines our fourth coupling approach. By construction, the relaxation system (66) under this condition is consistent with the coupled p-system given by (62) and (63). Unlike the previous approaches, this condition is nonlinear.

5.2 Riemann Solvers (RSs)

In this section, we analyze the RSs for the different coupling conditions considered in Sect. 5.1 and provide explicit forms for the implied coupling data.

Coupling approaches 1–3 The first three coupling conditions given by (66) and different choices for β_1 and β_2 fit into the linear framework discussed in Sect. 3.3 and correspond to

$$B_R = I, \qquad B_L = I, \qquad P = \big(0,\ \beta_1\mathcal{E},\ \beta_2\mathcal{E},\ 0\big)^{\mathrm{T}} \tag{70}$$

in the coupling function (31). To compute the coupling data from the RS, we conclude from Remark 2 that the system matrix in (34) is of the form

$$B := B_R\tilde{R}^- - B_L\tilde{R}^+ = -\begin{pmatrix} (\sqrt{A})^{-1} & (\sqrt{A})^{-1} \\ -I & I \end{pmatrix} = -\begin{pmatrix} \frac{1}{2}\sqrt{A} & -\frac{1}{2}I \\ \frac{1}{2}\sqrt{A} & \frac{1}{2}I \end{pmatrix}^{-1}, \tag{71}$$

from which we determine the parameters Σ^- and Σ^+ as

$$\begin{pmatrix} \Sigma^- \\ \Sigma^+ \end{pmatrix} = B^{-1}(P + Q_0^+ - Q_0^-), \qquad \Sigma^{\mp} = -\frac{1}{2}\sqrt{A}(P^U + U_0^+ - U_0^-) \pm \frac{1}{2}(P^V + V_0^+ - V_0^-). \tag{72}$$

Here $P^U = (0, \beta_1\mathcal{E})$ and $P^V = (\beta_2\mathcal{E}, 0)$ consist of the upper two and lower two entries in P, respectively. The trace data has the form

$$Q_0^{\mp} = \begin{pmatrix} U_0^{\mp} \\ V_0^{\mp} \end{pmatrix} = \begin{pmatrix} \rho_0^{\mp} & \rho_0^{\mp} v_0^{\mp} & V_{1,0}^{\mp} & V_{2,0}^{\mp} \end{pmatrix}^{\mathrm{T}}. \tag{73}$$

Eventually, the coupling data, for which we assume a notation analogue to (73), are given by (33) implying

$$\begin{cases} U_{\mathrm{R}} = \dfrac{1}{2}(U_0^- + U_0^+ + P^U) - \dfrac{1}{2}(\sqrt{A})^{-1}(V_0^+ - V_0^- + P^V), & \text{(74a)} \\ U_{\mathrm{L}} = \dfrac{1}{2}(U_0^- + U_0^+ - P^U) - \dfrac{1}{2}(\sqrt{A})^{-1}(V_0^+ - V_0^- + P^V), & \text{(74b)} \\ V_{\mathrm{R}} = \dfrac{1}{2}\sqrt{A}(U_0^- - U_0^+ - P^U) + \dfrac{1}{2}(V_0^+ + V_0^- + P^V), & \text{(74c)} \\ V_{\mathrm{L}} = \dfrac{1}{2}\sqrt{A}(U_0^- - U_0^+ - P^U) + \dfrac{1}{2}(V_0^+ + V_0^- - P^V). & \text{(74d)} \end{cases}$$

Due to Remark 3, which applies here since Ψ_Q is affine linear, the coupling data in the relaxation limit are determined by the same RS as in case of $\varepsilon > 0$. Thus, the data (74) also satisfies the coupling condition (66) in the limit $\varepsilon \to 0$.

Coupling approach 4 We next consider our fourth coupling approach, which introducing the notation $g^V(U_{\mathrm{L}}) = \mathcal{E}(0, (2\rho_{\mathrm{L}} v_{\mathrm{L}} + \mathcal{E})/\rho_{\mathrm{L}})^{\mathrm{T}}$ can be written as

$$\begin{pmatrix} U_{\mathrm{R}} \\ V_{\mathrm{R}} \end{pmatrix} = \begin{pmatrix} U_{\mathrm{L}} \\ V_{\mathrm{L}} \end{pmatrix} + \begin{pmatrix} P^U \\ P^V \end{pmatrix} + \begin{pmatrix} 0 \\ g^V(U_{\mathrm{L}}) \end{pmatrix}. \tag{75}$$

To obtain coupling data, we substitute the parametrization (24) and obtain

$$\begin{pmatrix} -(\sqrt{A})^{-1} \\ I \end{pmatrix} \Sigma^- - \begin{pmatrix} (\sqrt{A})^{-1} \\ I \end{pmatrix} \Sigma^+ - \begin{pmatrix} 0 \\ g^V(U_0^+ + (\sqrt{A})^{-1}\Sigma^+) \end{pmatrix} = \begin{pmatrix} U_0^+ - U_0^- + P^U \\ V_0^+ - V_0^- + P^V \end{pmatrix}. \tag{76}$$

From the first two components of (76), we get

$$\Sigma^- = \sqrt{A}(U_0^- - U_0^+ - P^U) - \Sigma^+, \tag{77}$$

which substituted into the components three and four in (76) yields

$$-2\Sigma^+ + \sqrt{A}(U_0^- - U_0^+ - P^U) - g^V(U_0^+ + (\sqrt{A})^{-1}\Sigma^+) = V_0^+ - V_0^- + P^V. \tag{78}$$

Using the notation $\Sigma^+ = (\sigma_1^+, \sigma_2^+)^{\mathrm{T}}$, we note that the first component of (78) determines σ_1^+, which in turn substituted into the second component of (78) determines σ_2^+. Eventually Σ^- is obtained from (77) and therefore an RS for approach four is defined. By the verified well-posedness of the RS and the differentiability of the corresponding coupling function, Remark 3 also applies to our fourth coupling approach and thus the above procedure also determines suitable coupling data in the relaxation limit.

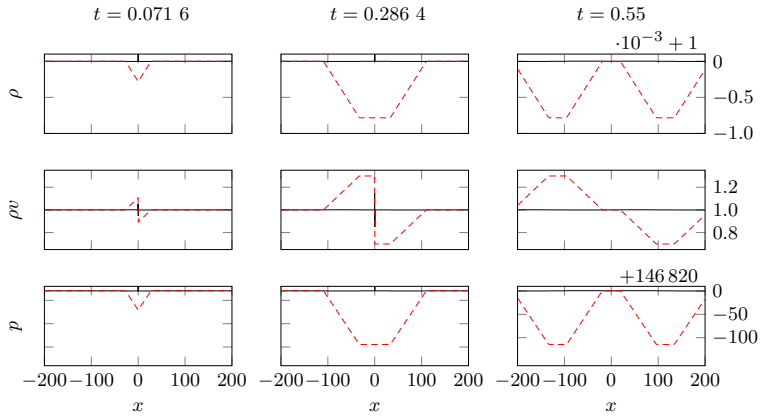

Fig. 3 Numerical solution for system (65) in the relaxation limit using coupling approach 1 given by (66), $\beta_1 = 1$ and $\beta_2 = 0$ (black line) compared to the reference solution (red dashed line). Peaks appear at the interface ($x = 0$). The coupled relaxed scheme on 1 000 mesh cells with CFL = 0.9 has been used

5.3 Numerical Experiments

We consider a numerical test case modified from [54, Sect. 5.2.1] employing constant initial data $\rho_0 = \rho_0 v_0 = 1$ and pressure given by $p(\rho) = 146\,820.4\rho$. As computational domain, we choose $[-200, 200]$ and impose homogeneous Neumann boundary conditions. The mass outtake at the interface is assumed time-dependent and given by

$$\mathcal{E}(t) = \begin{cases} \min\{0.6t, 3t\}, & \text{if } 0 \leqslant t < 0.3, \\ \max\{0, -3t + 1.5\}, & \text{if } t \geqslant 0.3. \end{cases} \tag{79}$$

A reference solution for the coupled p-system (62) and coupling condition (63) has been precomputed on a very fine grid consisting of 12 800 cells using an RS for the original problem developed in [54].

We employ the central scheme introduced in Sect. 4.2 to numerically compute solutions for system (65) in the limit $\varepsilon \to 0$ for the different coupling approaches considered in Sect. 5.1. For a numerical example demonstrating that the solution of the relaxation scheme converges to the one of the central scheme in the relaxation limit, we refer to [48]. In the numerical computations, we employ 1 000 uniform mesh cells and time increments chosen according to the CFL condition

$$\Delta t = \text{CFL}\frac{\Delta x}{\sqrt{a}}, \tag{80}$$

and the Courant number CFL = 0.9. Numerical results are presented in terms of the density, momentum, and pressure at the time instances $t = 0.071\,6$, 0.286 4, and 0.55.

In Fig. 3, we show results obtained by the first coupling approach given by (66), $\beta_1 = 1$ and $\beta_2 = 0$. In the numerical results, we see a peak in the density, momentum, and pressure forming and vanishing at the interface as time evolves. Comparing to the reference solution, this coupling condition imposed to the coupled relaxation system clearly cannot yield the solution of the original coupled p-system (62).

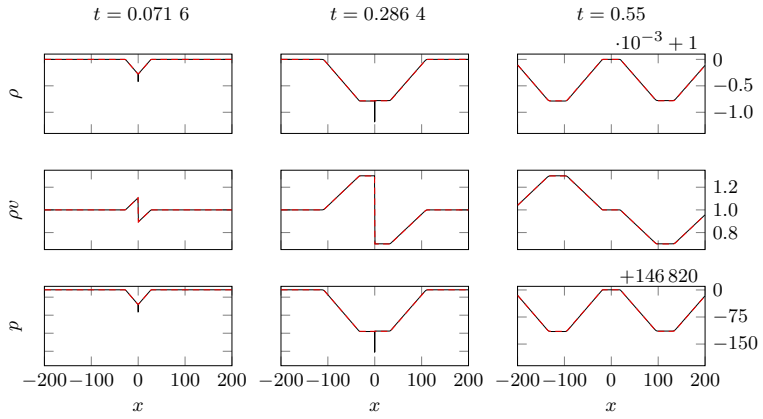

Fig. 4 Numerical solution for system (65) in the relaxation limit using coupling approach 2 given by (66), $\beta_1 = 0$ and $\beta_2 = 1$ (black line) compared to the reference solution (red dashed line). Artefacts at the interface ($x = 0$) are visible. The coupled relaxed scheme on 1 000 mesh cells with CFL = 0.9 has been used

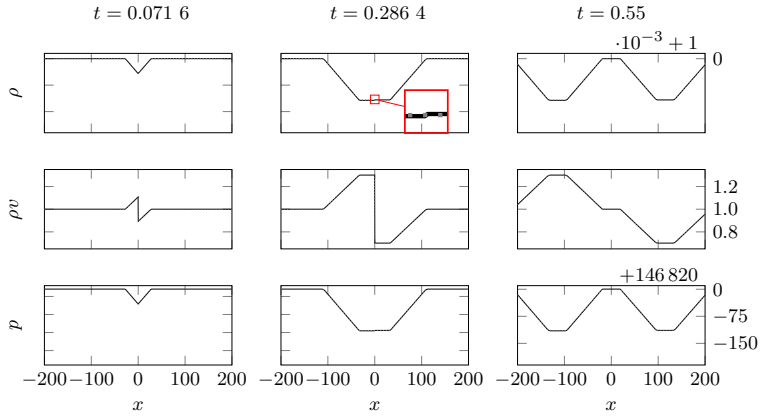

Fig. 5 Numerical solution for system (65) in the relaxation limit using coupling approach 3 (solid line) given by (66) and $\beta_1 = \beta_2 = 1$ and 4 (dotted line) given by (66a), (66b), (66c), (69) and $\beta_1 = \beta_2 = 1$. The coupled relaxed scheme on 1 000 mesh cells with CFL = 0.9 has been used. Except for a jump of small magnitude occurring in approach 3 at the interface, both solutions are indistinguishable

Figure 4 shows the numerical solution in case of the second coupling approach given by (66), $\beta_1 = 0$ and $\beta_2 = 1$. Whilst this solution qualitatively coincides with the reference solution for $x \neq 0$, it exhibits layer artefacts at the interface at the time instances 0.071 6 and 0.286 4.

Eventually, numerical results for the third coupling approach given by (66) and $\beta_1 = \beta_2 = 1$ are shown in Fig. 5. Using this condition, the solution of the coupled relaxation system qualitatively matches the one of the original system (62) with coupling condition (63). This indicates that the intrinsic contradiction in the relaxation limit between (66b) and (66c) in both coupling approaches 1 and 2 due to $\beta_1 \neq \beta_2$ deteriorates the quality of the relaxation approach as an approximation of the original problem.

Table 1 Mesh convergence in L^1 for the considered coupling approaches

Cells	Coupling 1	EOC	Coupling 2	EOC	Coupling 3	EOC	Coupling 4	EOC
100	1.794×10^{-1}		1.604×10^{-2}		1.238×10^{-2}		1.236×10^{-2}	
200	1.790×10^{-1}	0.00	8.495×10^{-3}	0.92	6.467×10^{-3}	0.94	6.449×10^{-3}	0.94
400	1.789×10^{-1}	0.00	4.404×10^{-3}	0.95	3.296×10^{-3}	0.97	3.247×10^{-3}	0.99
800	1.788×10^{-1}	0.00	2.451×10^{-3}	0.85	1.864×10^{-3}	0.82	1.691×10^{-3}	0.94
1 600	1.788×10^{-1}	0.00	1.425×10^{-3}	0.78	1.258×10^{-3}	0.57	8.447×10^{-4}	1.00
3 200	1.788×10^{-1}	0.00	1.064×10^{-3}	0.42	1.028×10^{-3}	0.29	4.122×10^{-4}	1.04

First-order error convergence is only indicated for coupling approach 4

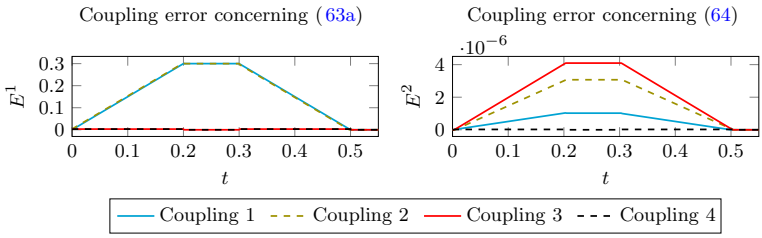

Fig. 6 Coupling errors E^1 (left) and E^2 (right) defined in (81) over the time interval [0, 0.55] for the four considered coupling approaches. Errors for numerical solutions computed by the central scheme on 1 000 mesh cells using CFL = 0.9 are considered. Both coupling approaches 3 and 4 achieve significantly lower errors than approaches 1 and 2 concerning (63a). Approach 4 reduces the error concerning (64) over approaches 1–3

We note hence, that consistency of the relaxation approach (65) to system (62) as we have verified for our fourth coupling approach has not been necessary to achieve an accurate numerical solution. This is presumably due to the small magnitude of the additional term $\mathcal{E}(2\rho_L v_L + \mathcal{E})/\rho_L$ in (69) that has been added in the fourth coupling approach, which compared to the magnitude of V_{2R} and V_{2L} is smaller by a factor of 10^{-6}. A magnification at the interface of the solution corresponding to approach 3 reveals a jump of low magnitude not present in the reference solution. The solution for the fourth coupling approach given by (66a), (66b), (66c), (69) and $\beta_1 = \beta_2 = 1$ also shown in Fig. 5 and being qualitatively almost similar to the one of coupling approach 3 does not exhibit this artefact and is indistinguishable from the reference solution.

In Table 1, we present the L^1 error for the considered coupling approaches after mesh refinement with respect to the reference solution along with the corresponding experimental order of convergence (EOC)[1]. The numerical solutions used in the error computations have been computed using the reduced Courant number CFL = 0.1 to reduce the

[1] The EOC is computed by the formula $\text{EOC} = \log_2(E_1/E_2)$ with E_1 and E_2 denoting the error in two consecutive lines of the table.

Table 2 Mesh convergence of the coupling error $L^1(E^1)$ over time for the considered coupling approaches

Cells	Coupling 1	EOC	Coupling 2	EOC	Coupling 3	EOC	Coupling 4	EOC
100	9.00×10^{-2}		9.13×10^{-2}		1.25×10^{-2}		1.25×10^{-2}	
200	9.00×10^{-2}	0.00	9.03×10^{-2}	0.02	6.27×10^{-3}	1.00	6.27×10^{-3}	1.01
400	9.00×10^{-2}	0.00	9.01×10^{-2}	0.00	3.13×10^{-3}	1.00	3.13×10^{-3}	1.01
800	9.00×10^{-2}	0.00	9.00×10^{-2}	0.00	1.57×10^{-3}	1.00	1.57×10^{-3}	1.00
1 600	9.00×10^{-2}	0.00	9.00×10^{-2}	0.00	7.84×10^{-4}	1.00	7.83×10^{-4}	1.00

First-order error convergence for approaches 3 and 4 is indicated

Table 3 Mesh convergence of the coupling error $L^1(E^2)$ over time for the considered coupling approaches

cells	Coupling 1	EOC	Coupling 2	EOC	Coupling 3	EOC	Coupling 4	EOC
100	3.13×10^{-7}		9.21×10^{-7}		1.23×10^{-6}		8.54×10^{-8}	
200	3.08×10^{-7}	0.02	9.21×10^{-7}	0.00	1.23×10^{-6}	0.00	4.27×10^{-8}	1.00
400	3.07×10^{-7}	0.01	9.21×10^{-7}	0.00	1.23×10^{-6}	0.00	2.13×10^{-8}	1.00
800	3.07×10^{-7}	0.00	9.21×10^{-7}	0.00	1.23×10^{-6}	0.00	1.07×10^{-8}	1.00
1 600	3.06×10^{-7}	0.00	9.21×10^{-7}	0.00	1.23×10^{-6}	0.00	5.34×10^{-9}	1.00

First-order error convergence is only indicated for approach 4

influence of temporal errors, which occur, in particular, due to the non-smoothness of the mass outtake (79) with respect to time. In case of coupling approach 1, no grid convergence is observed. Whilst in case of coupling approaches 3 and 4, the error decreases as the grid is refined the EOC reduces as higher grid resolutions are considered and the L^1 error stagnates. Using coupling approach 4, continuous first-order convergence can be clearly observed.

To evaluate the approximation of the original coupling condition, we analyze the numerical solutions at the coupling interface. Comparing the mass loss at the interface between the numerical simulations shown in Figs. 3–5 and the reference solution over the time interval [0, 0.55] yields 1.8×10^{-1} for approach 1 and 2×10^{-5} for approaches 2–4. Also with respect to mass loss over time, no difference between the approaches 2–4 can be seen. Furthermore, we consider the coupling errors with respect to the original coupling conditions (63a) and (64) defined as

$$E^1(t^n) = \left|(U^n_{-1} - U^n_0)_2 - \mathcal{E}\right|, \qquad E^2(t^n) = \left|(U^n_{-1} - U^n_0)_1\right|. \tag{81}$$

The coupling errors allow for an evaluation of the numerical solutions without reference solution. Using the numerical solutions by the central scheme over 1 000 mesh cells and employing the Courant number CFL = 0.9, we present these errors over time in Fig. 6. In case of the error concerning the density condition (64), the temporal errors follow the monotony of the mass outtake $\mathcal{E}$. Approaches 4 and 1 here yield lower errors than approaches 2 and 3. Concerning the momentum condition (63a), both approaches 1 and 2 yield coupling errors in the magnitude of the mass outtake and are clearly outperformed by approaches 3 and 4 both achieving similarly small errors.

To investigate the scaling of the coupling errors with the mesh resolution, we compute numerical solutions for increasing numbers of mesh cells and consider the errors (81) in the discrete L^1 norm over time, i.e.,

$$L^1(E^i) = \sum_{k=0}^{k_T} \Delta t E^i(t^k), \qquad k_T = \lceil \frac{0.55}{\Delta t} \rceil, \qquad i = 1, 2.$$

Table 2 shows the error $L^1(E^1)$ for the considered coupling approaches after mesh refinement along with the corresponding EOC. In case of coupling approaches 1 and 2, the errors are not significantly decreasing when refining the mesh. Conversely the mesh convergence of order one can be clearly observed for the coupling approaches 3 and 4.

The error $L^1(E^2)$ after mesh refinement is presented in Table 3. In case of the linear coupling approaches, no significant variation with the mesh resolution can be observed whilst the errors are of small magnitude. The convergence with respect to the mesh resolution is only observed in case of coupling approach 4 and consistency with the original problem. These results moreover justify the equivalence we require for the consistency in Definition 1, as an implication of the original coupling condition in coupling approach 3 has not been sufficient for the convergence at the interface whilst equivalence of Ψ_Q and Ψ_U at the relaxation limit in coupling approach 4 has resulted in the mesh convergence.

6 Conclusion

We have presented a novel framework to handle systems of conservation laws coupled at an interface using a relaxation approach. When systems of conservation laws are coupled, usually information on the Lax curves of the underlying systems as well as complex and error-prone computations are required to identify suitable coupling data. The relaxation approach avoids this complication by replacing the nonlinear systems of conservation laws by systems of linear balance laws. We have introduced RSs for the new approach, discussed their well-posedness and proposed a finite-volume scheme that can be generally applied to coupled hyperbolic problems.

The approach requires a suitable adjustment of the original coupling condition to account for the modified systems. Considering the p-system in a case study, we have illustrated how the choice of this condition affects the numerical solutions. Whilst accurate results could be obtained using simple linear ad-hoc conditions, best results that also exhibit convergence at the interface have been achieved constructing a coupling condition both leading to a well-defined RS and being in the relaxation limit consistent with the original coupling condition. Motivated by these results, we suggest the same strategy for the design of the relaxation coupling condition also for different coupled hyperbolic systems.

Acknowledgements The authors would like to thank A. Sikstel for providing the reference solution used in Sect. 5.3.

Funding Open Access funding enabled and organized by Projekt DEAL. The authors thank the Deutsche Forschungsgemeinschaft (DFG, German Research Foundation) for the financial support through 320021702/GRK2326, 333849990/IRTG-2379, B04, B05, and B06 of 442047500/SFB1481, HE5386/18-1, 19-2, 22-1, 23-1, 25-1, ERS SFDdM035 and under Germany's Excellence Strategy EXC-2023 Internet of Production 390621612 and under the Excellence Strategy of the Federal Government and the Länder. Support through the EU DATAHYKING is also acknowledged.

Data Availiability The source code used to produce the numerical experiments presented in this manuscript is available from the GitHub repository https://github.com/nklb/CentralNetworkScheme.

Compliance with Ethical Standards

Conflict of Interest On behalf of all authors, the corresponding author states that there is no conflict of interest.

Ethical Approval The authors state that they comply with the ethical standards.

References

1. Adimurthi, M.S., Veerappa Gowda, G.D.: Optimal entropy solutions for conservation laws with discontinuous flux-functions. J. Hyperbolic Differ. Equ. **2**(4), 783–837 (2005). https://doi.org/10.1142/S0219891605000622
2. Ambroso, A., Chalons, C., Coquel, F., Godlewski, E., Lagoutière, F., Raviart, P.-A., Seguin, N.: Coupling of general Lagrangian systems. Math. Comput. **77**(262), 909–941 (2008). https://doi.org/10.1090/S0025-5718-07-02064-9
3. Andreianov, B., Karlsen, K.H., Risebro, N.H.: A theory of L^1-dissipative solvers for scalar conservation laws with discontinuous flux. Arch. Ration. Mech. Anal. **201**(1), 27–86 (2011). https://doi.org/10.1007/s00205-010-0389-4
4. Banda, M.K., Häck, A.-S., Herty, M.: Numerical discretization of coupling conditions by high-order schemes. J. Sci. Comput. **69**(1), 122–145 (2016). https://doi.org/10.1007/s10915-016-0185-x
5. Banda, M.K., Herty, M., Klar, A.: Gas flow in pipeline networks. Netw. Heterog. Media **1**(1), 41–56 (2006). https://doi.org/10.3934/nhm.2006.1.41
6. Banda, M.K., Herty, M., Klar, A.: Coupling conditions for gas networks governed by the isothermal Euler equations. Netw. Heterog. Media **1**(2), 295–314 (2006). https://doi.org/10.3934/nhm.2006.1.295
7. Banda, M.K., Herty, M., Ngnotchouye, J.M.T.: On linearized coupling conditions for a class of isentropic multiphase drift-flux models at pipe-to-pipe intersections. J. Comput. Appl. Math. **276**, 81–97 (2015). https://doi.org/10.1016/j.cam.2014.08.021
8. Borsche, R.: Numerical schemes for networks of hyperbolic conservation laws. Appl. Numer. Math. **108**, 157–170 (2016). https://doi.org/10.1016/j.apnum.2016.01.006
9. Borsche, R., Kall, J.: ADER schemes and high order coupling on networks of hyperbolic conservation laws. J. Comput. Phys. **273**, 658–670 (2014). https://doi.org/10.1016/j.jcp.2014.05.042
10. Borsche, R., Klar, A.: Kinetic layers and coupling conditions for scalar equations on networks. Nonlinearity **31**(7), 3512–3541 (2018). https://doi.org/10.1088/1361-6544/aabc91
11. Bressan, A.: Hyperbolic Systems of Conservation Laws. Oxford Lecture Series in Mathematics and Its Applications, vol. 20, pp. 250. Oxford University Press, Oxford (2000). (**The one-dimensional Cauchy problem**)
12. Bressan, A., Čanić, S., Garavello, M., Herty, M., Piccoli, B.: Flows on networks: recent results and perspectives. EMS Surv. Math. Sci. **1**(1), 47–111 (2014). https://doi.org/10.4171/EMSS/2
13. Bretti, G., Natalini, R., Piccoli, B.: Fast algorithms for the approximation of a traffic flow model on networks. Discret. Contin. Dyn. Syst. Ser. B **6**(3), 427–448 (2006). https://doi.org/10.3934/dcdsb.2006.6.427
14. Brouwer, J., Gasser, I., Herty, M.: Gas pipeline models revisited: model hierarchies, nonisothermal models, and simulations of networks. Multiscale Model. Simul. **9**(2), 601–623 (2011). https://doi.org/10.1137/100813580

15. Bürger, R., Karlsen, K.H., Klingenberg, C., Risebro, N.H.: A front tracking approach to a model of continuous sedimentation in ideal clarifier-thickener units. Nonlinear Anal. Real World Appl. **4**(3), 457–481 (2003). https://doi.org/10.1016/S1468-1218(02)00071-8
16. Chalons, C., Raviart, P.-A., Seguin, N.: The interface coupling of the gas dynamics equations. Q. Appl. Math. **66**(4), 659–705 (2008). https://doi.org/10.1090/S0033-569X-08-01087-X
17. Chapman, S., Cowling, T.G.: The Mathematical Theory of Non-Uniform Gases: an Account of the Kinetic Theory of Viscosity, Thermal Conduction, and Diffusion in Gases. Cambridge Mathematical Library, 3rd edn. Cambridge University Press, Cambridge, New York (1990)
18. Chertkov, M., Fisher, M., Backhaus, S., Bent, R., Misra, S.: Pressure fluctuations in natural gas networks caused by gas-electric coupling. In: 2015 48th Hawaii International Conference on System Sciences, pp. 2738–2747 (2015). https://doi.org/10.1109/hicss.2015.330
19. Coclite, G.M., Garavello, M.: Vanishing viscosity for traffic on networks. SIAM J. Math. Anal. **42**(4), 1761–1783 (2010). https://doi.org/10.1137/090771417
20. Colombo, R.M., Herty, M., Sachers, V.: On 2×2 conservation laws at a junction. SIAM J. Math. Anal. **40**(2), 605–622 (2008). https://doi.org/10.1137/070690298
21. Colombo, R.M., Mauri, C.: Euler system for compressible fluids at a junction. J. Hyperbolic Differ. Equ. **5**(3), 547–568 (2008). https://doi.org/10.1142/S0219891608001593
22. Coquel, F., Jin, S., Liu, J.-G., Wang, L.: Well-posedness and singular limit of a semilinear hyperbolic relaxation system with a two-scale discontinuous relaxation rate. Arch. Ration. Mech. Anal. **214**(3), 1051–1084 (2014). https://doi.org/10.1007/s00205-014-0773-6
23. D'Apice, C., Göttlich, S., Herty, M., Piccoli, B.: Modeling, Simulation, and Optimization of Supply Chains, pp. 206. Society for Industrial and Applied Mathematics (SIAM), Philadelphia (2010). https://doi.org/10.1137/1.9780898717600. (**A continuous approach**)
24. Diehl, S.: On scalar conservation laws with point source and discontinuous flux function. SIAM J. Math. Anal. **26**(6), 1425–1451 (1995). https://doi.org/10.1137/S0036141093242533
25. Dubois, F., Le Floch, P.: Boundary conditions for nonlinear hyperbolic systems of conservation laws. J. Differential Equations **71**(1), 93–122 (1988). https://doi.org/10.1016/0022-0396(88)90040-X
26. Egger, H.: A robust conservative mixed finite element method for isentropic compressible flow on pipe networks. SIAM J. Sci. Comput. **40**(1), 108–129 (2018). https://doi.org/10.1137/16M1094373
27. Formaggia, L., Nobile, F., Quarteroni, A., Veneziani, A.: Multiscale modelling of the circulatory system: a preliminary analysis. Comput. Vis. Sci. **2**(2/3), 75–83 (1999). https://doi.org/10.1007/s007910050030
28. Garavello, M., Han, K., Piccoli, B.: Models for vehicular traffic on networks. In: AIMS Series on Applied Mathematics, vol. 9, pp. 474. American Institute of Mathematical Sciences (AIMS), Springfield (2016)
29. Garavello, M., Piccoli, B.: Traffic Flow on Networks: Conservation Law Models. In: AIMS Series on Applied Mathematics, vol. 1. American Inst. of Mathematical Sciences, Springfield (2006)
30. Gimse, T., Risebro, N.H.: Solution of the Cauchy problem for a conservation law with a discontinuous flux function. SIAM J. Math. Anal. **23**(3), 635–648 (1992). https://doi.org/10.1137/0523032
31. Godlewski, E., Raviart, P.-A.: The numerical interface coupling of nonlinear hyperbolic systems of conservation laws: I. The scalar case. Numer. Math. **97**(1), 81–130 (2004). https://doi.org/10.1007/s00211-002-0438-5
32. Godlewski, E., Raviart, P.-A.: A method of coupling non-linear hyperbolic systems: examples in CFD and plasma physics. Int. J. Numer. Methods Fluids **47**(10/11), 1035–1041 (2005). https://doi.org/10.1002/fld.856. (**8th ICFD Conference on Numerical Methods for Fluid Dynamics. Part 2**)
33. Hantke, M., Müller, S.: Analysis and simulation of a new multi-component two-phase flow model with phase transitions and chemical reactions. Q. Appl. Math. **76**(2), 253–287 (2018). https://doi.org/10.1090/qam/1498
34. Hantke, M., Müller, S.: Closure conditions for a one temperature non-equilibrium multi-component model of Baer-Nunziato type. ESAIM Proc. Surv. **66**, 42–60 (2019). https://doi.org/10.1051/proc/201966003
35. Herty, M., Jörres, C., Piccoli, B.: Existence of solution to supply chain models based on partial differential equation with discontinuous flux function. J. Math. Anal. Appl. **401**(2), 510–517 (2013). https://doi.org/10.1016/j.jmaa.2012.12.002
36. Herty, M., Kolbe, N., Müller, S.: Central schemes for networked scalar conservation laws. Netw. Heterog. Media **18**(1), 310–340 (2023). https://doi.org/10.3934/nhm.2023012
37. Herty, M., Mohring, J., Sachers, V.: A new model for gas flow in pipe networks. Math. Methods Appl. Sci. **33**(7), 845–855 (2010). https://doi.org/10.1002/mma.1197

38. Herty, M., Müller, S., Sikstel, A.: Coupling of compressible Euler equations. Vietnam J. Math. **47**(4), 769–792 (2019). https://doi.org/10.1007/s10013-019-00353-7
39. Herty, M., Rascle, M.: Coupling conditions for a class of second-order models for traffic flow. SIAM J. Math. Anal. **38**(2), 595–616 (2006). https://doi.org/10.1137/05062617X
40. Holden, H., Risebro, N.H.: A mathematical model of traffic flow on a network of unidirectional roads. SIAM J. Math. Anal. **26**(4), 999–1017 (1995). https://doi.org/10.1137/S0036141093243289
41. Holle, Y., Herty, M., Westdickenberg, M.: New coupling conditions for isentropic flow on networks. Netw. Heterog. Media **15**(4), 605–631 (2020). https://doi.org/10.3934/nhm.2020016
42. Hu, J., Jin, S., Li, Q.: Asymptotic-preserving schemes for multiscale hyperbolic and kinetic equations. In: Handbook of Numerical Analysis, vol. 18, pp. 103–129. Elsevier, Amsterdam (2017). https://doi.org/10.1016/bs.hna.2016.09.001
43. Jin, S., Liu, J.-G., Wang, L.: A domain decomposition method for semilinear hyperbolic systems with two-scale relaxations. Math. Comput. **82**(282), 749–779 (2013). https://doi.org/10.1090/S0025-5718-2012-02643-3
44. Jin, S., Xin, Z.: The relaxation schemes for systems of conservation laws in arbitrary space dimensions. Commun. Pure Appl. Math. **48**(3), 235–276 (1995). https://doi.org/10.1002/cpa.3160480303
45. Karlsen, K.H., Klingenberg, C., Risebro, N.H.: A relaxation scheme for conservation laws with a discontinuous coefficient. Math. Comput. **73**(247), 1235–1260 (2003). https://doi.org/10.1090/S0025-5718-03-01625-9
46. Karlsen, K.H., Towers, J.D.: Convergence of a Godunov scheme for conservation laws with a discontinuous flux lacking the crossing condition. J. Hyperbolic Differ. Equ. **14**(04), 671–701 (2017). https://doi.org/10.1142/S0219891617500229
47. Kolb, O., Lang, J., Bales, P.: An implicit box scheme for subsonic compressible flow with dissipative source term. Numer. Algorithms **53**(2/3), 293–307 (2010). https://doi.org/10.1007/s11075-009-9287-y
48. Kolbe, N.: Numerical relaxation limit and outgoing edges in a central scheme for networked conservation laws. PAMM **23**(1), 202200150 (2023). https://doi.org/10.1002/pamm.202200150
49. Liu, T.-P.: Hyperbolic conservation laws with relaxation. Commun. Math. Phys. **108**(1), 153–175 (1987). https://doi.org/10.1007/BF01210707
50. Mishra, S.: Numerical methods for conservation laws with discontinuous coefficients. In: Handbook of Numerical Analysis, vol. 18, pp. 479–506. Elsevier, Amsterdam (2017). https://doi.org/10.1016/bs.hna.2016.11.002
51. Müller, L.O., Blanco, P.J.: A high order approximation of hyperbolic conservation laws in networks: application to one-dimensional blood flow. J. Comput. Phys. **300**, 423–437 (2015). https://doi.org/10.1016/j.jcp.2015.07.056
52. Müller, S., Voss, A.: The Riemann problem for the Euler equations with nonconvex and nonsmooth equation of state: construction of wave curves. SIAM J. Sci. Comput. **28**(2), 651–681 (2006). https://doi.org/10.1137/040619909
53. Reigstad, G.A., Flåtten, T., Erland Haugen, N., Ytrehus, T.: Coupling constants and the generalized Riemann problem for isothermal junction flow. J. Hyperbolic Differ. Equ. **12**(1), 37–59 (2015). https://doi.org/10.1142/S0219891615500022
54. Sikstel, A.: Analysis and numerical methods for coupled hyperbolic conservation laws. Dissertation, RWTH Aachen University, Aachen (2020). https://doi.org/10.18154/RWTH-2020-07821
55. Towers, J.D.: An explicit finite volume algorithm for vanishing viscosity solutions on a network. Netw. Heterog. Media **17**(1), 1 (2022). https://doi.org/10.3934/nhm.2021021
56. Zlotnik, A., Roald, L., Backhaus, S., Chertkov, M., Andersson, G.: Control policies for operational coordination of electric power and natural gas transmission systems. In: 2016 American Control Conference (ACC), pp. 7478–7483 (2016). https://doi.org/10.1109/ACC.2016.7526854